High-*Q* plasmonic infrared absorber for sensing of molecular resonances in hybrid lead halide perovskites

Govind Dayal,[1,2] Ankur Solanki,[1] Xin Yu Chin,[1] Tze Chien Sum,[1] Cesare Soci,[1,2] and Ranjan Singh[1,2,a)]

[1]*Division of Physics and Applied Physics, School of Physical and Mathematical Sciences, Nanyang Technological University, 21 Nanyang Link, Singapore 637371*

[2]*Center for Disruptive Photonic Technologies, The Photonic Institute, Nanyang Technological University, 50 Nanyang Avenue, Singapore 639798*

(Received 27 April 2017; accepted 18 July 2017; published online 17 August 2017)

Plasmonic resonances in sub-wavelength metal-dielectric-metal cavities have been shown to exhibit strong optical field enhancement. The large field enhancements that occur in sub-wavelength regions of the cavity can drastically boost the performance of microcavity based detectors, electromagnetic wave absorbers, metasurface hologram, and nonlinear response of the material in a cavity. The performance efficiencies of these plasmonic devices can be further improved by designing tunable narrow-band high-*Q* cavities. Here, we experimentally and numerically demonstrate high-*Q* resonances in metal-dielectric-metal cavity consisting of an array of conductively coupled annular and rectangular apertures separated from the bottom continuous metal film by a thin dielectric spacer. Both, the in-plane and out of plane coupling between the resonators and the continuous metal film have been shown to support fundamental and higher order plasmonic resonances which result in high-*Q* response at mid-infrared frequencies. As a sensor application of the high-*Q* cavity, we sense the vibrational resonances of an ultrathin layer of solution-processed organic–inorganic hybrid lead halide perovskites. *Published by AIP Publishing.*
[http://dx.doi.org/10.1063/1.4997442]

I. INTRODUCTION

The resonant interaction of light with metal nanostructures can result in extraordinary optical effects in both the near and far fields. It is well known that the optical properties of metallic nanostructures are closely related to their shape, size, composition, and the surrounding dielectric environment.[1–3] The spectral position of the resonance is mainly governed by the size and shape of the nanostructure, and the linewidth of the resonance is governed by the losses present in the system. The resonant structures possess two kinds of losses: radiative (Γ_r) and non-radiative (Γ_{nr}).[4,5] Non-radiative losses in metallic nanostructures are related to the lifetimes of all electron scattering processes which are mainly electron-electron, electron-phonon, and electron-defect scattering of the bulk material. Radiative losses, on the other hand, arise due to the sub-wavelength nature of the resonant nanostructures. The radiation efficiencies of nanostructures depend on eigenmode resonances such as dipole, quadrupole, and higher order modes. The fundamental dipolar mode of a nanostructure radiates efficiently and is classified as a super-radiant in contrast to higher order modes, which are not easily excited by light at normal incidence and have poor radiative efficiencies. However, it has been demonstrated that the higher order modes of a resonator can be excited indirectly through near-field coupling to the optically excited dipole mode of another resonator placed nearby, or by breaking the structural symmetry. Due to the smaller radiative losses, higher order plasmonic modes have narrower linewidths in comparison to the dipole mode. Thus, by engineering the structural parameters of a nanostructure to select a particular plasmonic mode, one can control the radiative loss in the system and hence the linewidth of the resonant spectrum. Moreover, interference between the dipole and higher order modes gives rise to sharp Fano resonance in the scattering spectrum which has an asymmetric line shape.[6–8]

Another efficient method of controlling the radiative loss in a plasmonic system is the coupling of nanoparticle with a metallic film.[9–11] When a nanoparticle is brought in close proximity of a metallic thin film, the charge distribution on the nanoparticle induces image charges in the metallic film. For a dipole aligned parallel to the film, the image dipole is in the opposite direction, and the net dipole moment of the composite medium is reduced, which reduces radiative damping causing the spectral narrowing of dipolar plasmon linewidth. The strength of the image dipole is strongly dependent on the thickness and the dielectric constant of the spacer material. Therefore, the dielectric material placed between the resonators and its refractive index plays a vital role in controlling the radiative loss (Γ_r) of the composite system. Thus, the radiative loss of a metal-dielectric-metal composite medium is a function of the dipole moment (p) of the nanoparticle, the dipole moment of image charge (p_i), refractive index (n_d) and thickness of the dielectric spacer (h). The control of dielectric film thickness provides an easy method to precisely tune the radiative loss of the system. Controlling the radiative loss of a system determines the resonance line width of the nanostructures. The reflection coefficient of the ground plane terminated metasurface can be expressed using the coupled mode theory as

a)Author to whom correspondence should be addressed: ranjans@ntu.edu.sg

$$r(\omega) = \frac{(\Gamma_r - \Gamma_{nr}) - i(\omega - \omega_0)}{(\Gamma_r - \Gamma_{nr}) + i(\omega - \omega_0)},$$

where ω_0 is the resonant frequency of the eigenmode and Γ_r, Γ_{nr} represent the radiative and the resistive losses, respectively.[10]

Critical coupling occurs when the radiative and non-radiative losses of the cavity are equal, i.e., $\Gamma_r = \Gamma_{nr}$. For a critically coupled plasmonic system, an incoming field excites the eigenmode through the radiative coupling and the incoming energy is transformed into resistive loss without causing any reflection.[12] In the ideal case, no energy is back-reflected or transmitted. It is a general concept which finds applications in a vast range of fields, such as microcavity based detectors,[12] perfect absorbers,[13] metasurface holograms,[14] and nonlinear response.[15,16] Perfect absorption has been demonstrated in several metallic structures including a metal-dielectric-metal cavity, surface lattice mode based resonances,[17] and plasmonic cavities.[13] A tri-layer metal-dielectric-metal, composite medium with a top film consisting of an array of sub-wavelength size resonators, can exhibit perfect absorption at predictable wavelengths, corresponding to simultaneous excitation of the electric and the magnetic resonance in the metal-dielectric-metal cavity.[18–20]

The infrared frequency band of the electromagnetic spectrum is of particular interest for sensing due to the spectroscopic features associated with molecular resonances found throughout these regions. Metamaterial-based infrared absorbers have been designed and demonstrated for applications in chemical and biological sensing, thermal imaging, astronomy, night vision, and pollution monitoring.[13] The performance of metamaterial-based devices for all these applications can be enormously increased by tunable high-Q near perfect metamaterial absorbers. The lattice mode based designs give rise to sharp resonances but they are not in the sub-wavelength regime.[17] Thus, the quest for the tunable narrow band high-Q absorber in sub-wavelength sized metamaterial cavity is still ongoing.

In this work, we propose and demonstrate a high-Q metamaterial absorber at mid-infrared frequencies. Our proposed design consists of a tri-layer metal-dielectric-metal composite medium with top film perforated with an array of conductively coupled annular and rectangular aperture arrays that can support high-Q resonances. Both the in-plane between the resonators and the out of plane coupling resonators and metallic ground plane are investigated to tailor the optical response of the cavity. As a proof of principle, high-Q cavity resonances are utilized to sense the vibrational resonance modes of solution-processed hybrid organic–inorganic perovskite methylammonium iodide with chemical formula $CH_3NH_3PbI_3$.

II. RESULTS AND DISCUSSION

The schematic diagram of the proposed structure is depicted in Fig. 1 with a magnified unit cell shown in the inset. In this figure, R_i and R_o indicate the inner and outer radius of the annular aperture, respectively, and l is the length of the rectangular aperture. To study the coupling

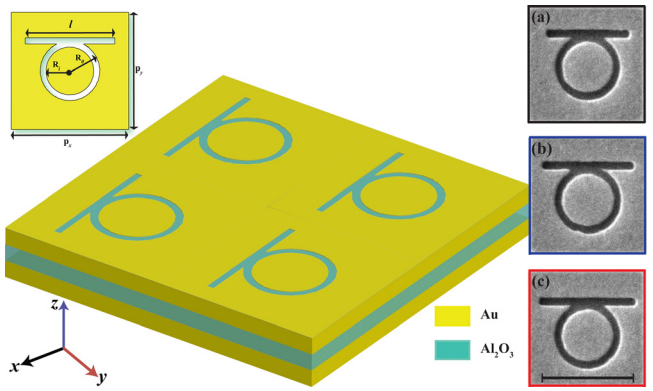

FIG. 1. Schematic diagram of the proposed metal-dielectric-metal cavity consisting of overlapping annular and rectangular apertures array on top. The SEM images of the unit cell of the fabricated samples are shown in (a)–(c). The length of the rectangular apertures shown in (a), (b), and (c) are 1.4, 1.5, and 1.6 μm, respectively, and the inner and outer radius of the annular apertures are R_i= 390 nm and R_0= 525 nm. The scale bar equals 1.5 μm.

between the annular and rectangular aperture, we fabricated arrays of connected annular and rectangular aperture structures with varying length of the rectangular aperture. The inner and outer radius of the annular aperture were kept constant to be 390 and 525 nm, respectively, for all the arrays shown in Fig. 1. The overlap distance between the individual annular aperture and rectangular aperture has also been kept constant for all the structures. The thicknesses of the top gold layer and Al_2O_3 are 80 and 50 nm, respectively. The scanning electron microscopy (SEM) images of the fabricated overlapping annular and rectangular apertures, demonstrating the high quality of the well-defined patterns, are shown in Figs. 1(a)–1(c).

In Figs. 2(a) and 2(c), we plot the measured spectra of the three representative structures shown in Figs. 1(a)–1(c), for two orthogonal polarizations. The measured reflection spectrum [black curve in Fig. 2(a)] obtained from the overlapping annular and rectangular aperture arrays with $l = 1.4$ μm shows a symmetric dip at 3.27 μm and three asymmetric line-shape dips at 3.67, 3.95, and 4.35 μm, respectively. The symmetric resonance dip at 3.27 μm ($Q = 11$), is due to excitation of the dipolar resonance in the annular aperture, while the asymmetric line shape Fano resonances at 3.67, 3.95, and 4.35 μm, with quality factors of 27, 38, and 20 arise due to the near-field interaction and hybridization between the plasmon modes of coupled annular and rectangular apertures. The quality factors of the dipole and Fano resonances were calculated using $Q = \lambda_r/\delta\lambda$, where λ_r is the resonance wavelength and $\delta\lambda$ is the full width at half maxima. When the polarization of the incident wave is changed from x- to y-polarization, the measured spectrum [magenta curve in Fig. 2(c)] shows two symmetric dips at 3.27 and 5.35 μm and two asymmetric line-shaped dips at 3.66 and 3.98 μm, respectively. We observe that the amplitude of the Fano resonances for y-polarization is relatively smaller than the amplitude of the Fano resonances for the x-polarization. Next, we consider the reflection spectra of the overlapping annular and rectangular aperture arrays having the aperture length l of 1.5 μm and 1.6 μm, the measured reflection spectra show similar behavior as that for $l = 1.4$ μm for both the polarizations but with a slight red shift

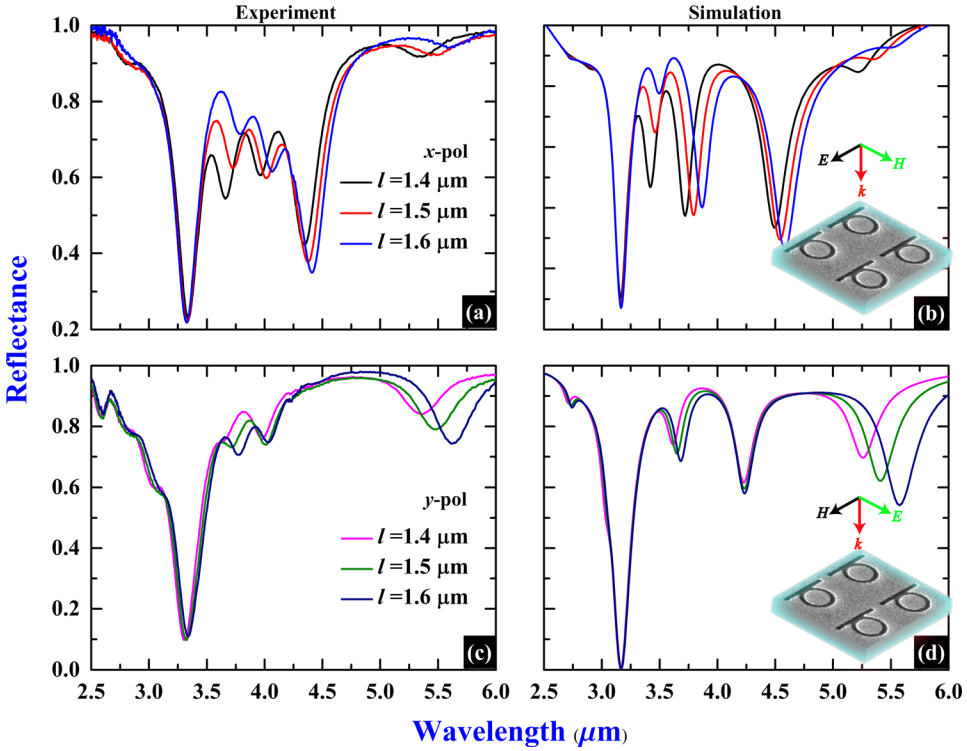

FIG. 2. Experimental and simulated reflection spectra of the three metamaterials with $l = 1.4$, 1.5, and 1.6 μm as shown in Figs. 1(a)–1(c). The incident electric field is polarized in the x-direction (parallel to the long axis of the rectangle) and the y-direction (perpendicular to the long axis of the rectangle) as shown in the insets.

in the spectral position of the Fano resonances which are generated through the hybridization between the plasmon modes of annular and rectangular apertures. We also find that as the length of the rectangular aperture increases, the amplitude of the reflection decreases which is attributed to better impedance matching of the composite medium with the free space.

In order to analyze the underlying physics of the observed resonant coupling, simulations were performed using a finite element method based commercial software COMSOL Multiphysics. The simulated reflection spectra of the three arrays for both polarizations have been shown in Figs. 2(b) and 2(d) that match well with the corresponding experimental spectra shown in Figs. 2(a) and 2(c). The electric and magnetic field distributions calculated at the respective dip positions in the reflection spectrum [black curve of Fig. 2(b) and magenta curve of Fig. 2(d)] provide insight into the underlying plasmon modes of the composite metamaterials. As shown in Fig. 3(a), the electric and magnetic field distribution plots at 3.17 μm manifest the excitation of the dipolar plasmon resonance in the annular aperture with the strongly confined field in the annular gaps. These plasmon modes excited in the annular apertures are plasmonic whispering gallery modes with different azimuthal mode number ($m = 0$, 1, 2,….).[21,22] The electric field distribution plots at 3.42 μm and 3.72 μm display the excitation of dipolar resonance in the annular aperture ($m = 1$) and dipolar and quadrupolar resonances in the rectangular aperture, respectively. The excitation and interference of the dipolar and quadrupolar modes of the rectangular aperture with the dipolar mode ($m = 1$) of annular aperture confirm that the reflection dips at 3.42 μm and 3.72 μm observed for x-polarization are Fano resonances. Similarly, for y-polarization, the reflection dip at 3.17 μm is due to the collective excitation of dipolar plasmon resonance ($m = 1$) in the annular aperture and the dips at 3.62 μm and 4.42 μm are due to the interference of the $m = 0$ and $m = 1$ modes of the annular aperture with the dipolar mode of rectangular aperture as shown in Figs. 3(f) and 3(g), respectively. From the measured and simulated spectra shown in Fig. 2, we observe that the resonance frequency (3.17 μm) of dipolar mode of the annular aperture for the x- and y-polarizations is independent of the length of the rectangular aperture and appear to be at the same wavelength due to symmetrical nature of annular aperture. The magnetic field distribution plots at Fano resonances reveal strong localization of magnetic field near the edges of the rectangular aperture which suggest that a small change in the aperture length will influence the overall resonance position of the hybridized modes and the Fano resonances excited due to the interference of plasmon modes can be tuned through the variation in rectangular aperture's length. The electric field distribution plot at 5.25 μm indicates the excitation of a delocalized plasmon mode of the annular aperture which can be seen in both the measured and simulated spectra of the structure for both x- and y-polarizations show a strong dependence on the length of the rectangular aperture. The slight mismatch between the experimental and numerical simulation is attributed to the fabrication imperfections and the assumption of non-dispersive dielectric constant ($n = 1.7$) of Al_2O_3 in the numerical simulation.

III. SENSING OF THE VIBRATIONAL RESONANCE MODES OF HYBRID PEROVSKITE

In this section, we discuss the possibility of enhancing the molecular absorption of ultrathin film perovskite over layer using high-Q metal-dielectric-metal cavity. Solution-processed hybrid organic–inorganic perovskites with

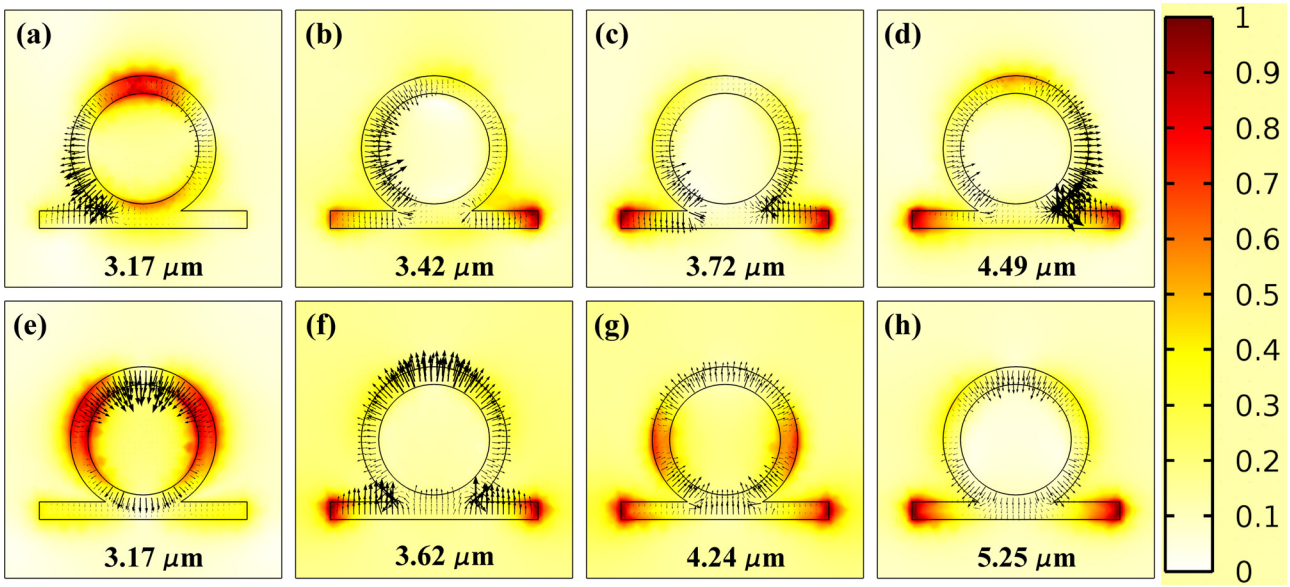

FIG. 3. Simulated electric field (black arrows) and magnetic field (color contour plot) distribution on the top surface of the metamaterial at respective dip positions in the reflection spectra for the *x*-polarization (top panels) and the *y*-polarization (bottom panels). The arrows represent the vectors of the electric field and the color contour plot indicates the normalized magnetic field.

formula $CH_3NH_3PbX_3$ (X = Cl, Br, I) exhibit a rich structural and electronic behavior that is strongly influenced by the complex interactions between the organic and inorganic subunits.[23–25] Lead–halide HOIPs have recently emerged as highly efficient optoelectronic materials and are being intensively investigated and developed for photovoltaics (PVs), photodetection, light-emitting diodes, and laser devices.[26,27] Perovskite ($CH_3NH_3PbI_3$) has several infrared absorption bands in the mid-infrared range. We choose two absorption bands at 2712 cm^{-1} (3.687 μm) and 3132 cm^{-1} (3.192 μm) which correspond to coupled vibration mode of symmetric NH_3 bend and CH_3-NH_3 rock and symmetric NH_3 stretch, respectively.[28,29] Pérez-Osorio *et al.* have investigated the vibrational properties of the hybrid organic/inorganic halide perovskite $CH_3NH_3PbI_3$ by first-principles density-functional perturbation theory calculations to obtain the relative infrared intensities of the vibrational modes. The infrared intensities of symmetric NH_3 bend, CH_3-NH_3 rock, and symmetric NH_3 stretch modes calculated using the DFT calculation were found to be 2.4, 0.1, and 5 $(D/Å)^2$/amu, respectively.[28] The absorption band at 2712 cm^{-1} is relatively weaker than the absorption band at 3132 cm^{-1}. Both of these modes are not detectable in the infrared spectra of a 60 nm thin film ($\lambda/50$) perovskite coated on a quartz substrate as shown in Fig. 4(b) (green curve) and need strong field enhancement to be detected.[30–34] Hence, to study the plasmon-vibrational mode coupling, which is maximum when plasmon mode and vibrational mode spectrally overlap, we fabricated two new absorber sensors to match the dipole resonance of the annular aperture with the absorption band of $CH_3NH_3PbI_3$ at 2712 cm^{-1} and 3132 cm^{-1}. The SEM image of the fabricated metamaterials reveals elliptical nature of the inner disks. The outer radius of the annular hole and length of the slit for metamaterial, fabricated to match the vibrational mode at 3132 cm^{-1}, are measured to be 500 nm and 1.3 μm, respectively, and the semi major axis and semi minor axis of the inner disk are 390 and 350 nm, respectively. For the other metamaterial design, the outer radius of the annular hole and length of the slit are taken to be 475 nm and 1.3 μm, respectively, and the semi major axis and semi minor axis of the disk were measured to be 365 and 325 nm, respectively. As shown in Fig. 4(a), the absorption at 2750 cm^{-1} (slightly shifted from its original position at 2712 cm^{-1}) can be only seen in the infrared spectra of the 60 nm thin perovskite coated on top of metamaterial sensor when the reflection dip of the dipole resonances matches with the vibrational mode (magenta curve). When the dipole resonance of the annular aperture is detuned by changing the incidence polarization to *y-pol*, the absorption peak can hardly be seen (black curve). This indicates that vibrational mode observed for *x-pol* is result of strong interaction of the plasmonic resonances with molecular dipoles. This is due to the fact that interaction strength ($H_{int} = -p_m \cdot E_l$) is maximum when both the resonance are at the same frequency and reduces drastically as the local field enhancement (E_l ($\lambda \neq \lambda_r$) < E_l (λ_r)) is reduced at non-resonant frequencies. Thus, if the dipole strength (p_m) of a vibrational mode is weak, one would need a high-Q plasmonic resonance and consequently high local field enhancement, to enhance the absorption level of the vibrational mode for the detection and quantification of very low volume of a target analyte. On the other hand, the vibrational mode at 3204 cm^{-1} (shifted from its original position at 3132 cm^{-1}) which is a strong vibrational mode, can be clearly seen in detuned spectra of perovskite coated metamaterial for both the polarizations owing to its relatively strong oscillator strength as shown in Fig. 4(b). Coupling between the plasmonic resonance and vibrational mode not only leads to the amplification of the absorption level of the vibrational mode but also leads to formation of new states that are strongly dependent on the linewidth of the plasmonic resonance and the molecular strength of the vibrational mode.

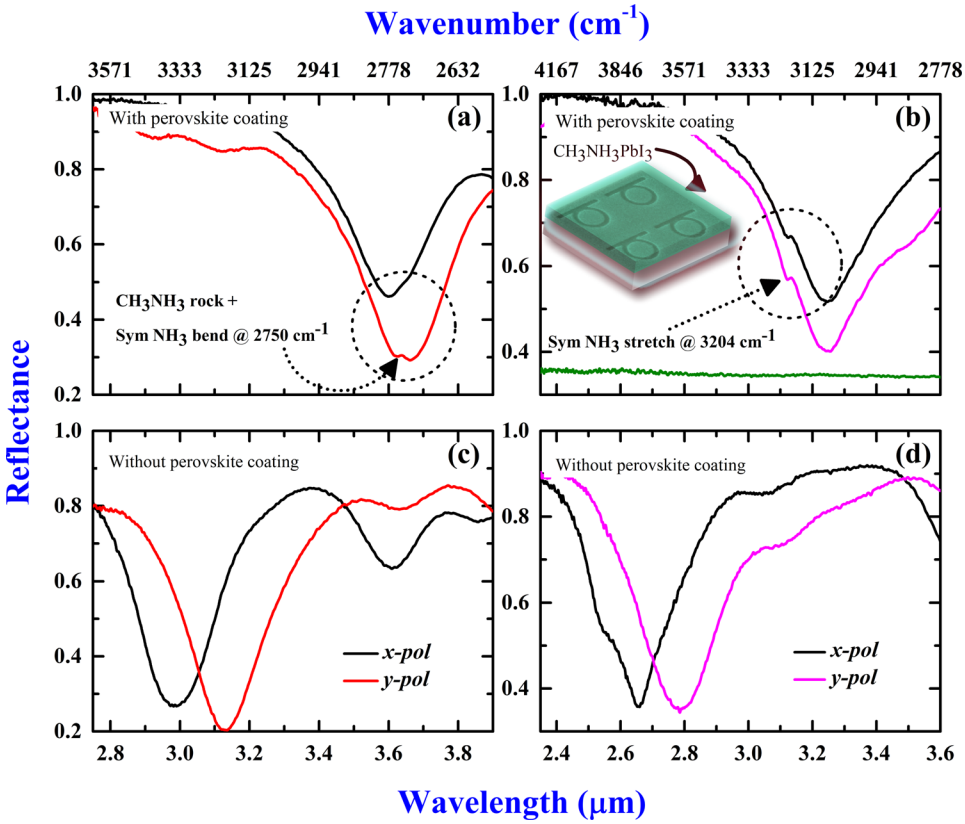

FIG. 4. (a) and (b) Measured reflectance spectra of the two metamaterials after the coating of 60 nm thin perovskite coating for *x*- and *y*-polarizations. The enhanced absorption at 2750 cm^{-1} and at 3204 cm^{-1} can be seen in (a) and (b). The reflection spectra of the bare metamaterial samples having specific geometrical parameters: $R_i = 350$ nm, $R_0 = 500$ nm, and $l = 1.3\,\mu$m and $R_i = 325$ nm, $R_0 = 475$ nm and $l = 1.3\,\mu$m, respectively, are shown in (c) and (d).

The measured reflection spectra of the plasmonic absorber sensor prior to the perovskite coating are shown in Figs. 4(c) and 4(d) for both the polarizations. Comparing the reflection spectra obtained before and after perovskite coating, we find that red shifts in the resonance position of dipole mode caused by the perovskite are different for two orthogonal polarizations which are due to the elliptical nature of the annular aperture. To investigate the distinct shift for two polarizations shown in Figs. 4(a) and 4(c), we carried out numerical simulations of the metamaterial with and without perovskite coating by taking the elliptical nature of the annular aperture into consideration. In the simulation, the thickness and refractive index of the perovskite film are taken to be 60 nm and 2.2, respectively. The simulated spectra before (solid lines) and after perovskite coating (dotted lines) for both polarizations are shown in Fig. 1 of supplementary materials. The distinct frequency shift observed in the experiment can clearly be seen in the simulation. It is worth mentioning here that the high sensitivity of the perovskite coated metamaterial is due to the filling of annular gaps with perovskite, which is extremely sensitive to local changes in refractive index.

Recently, it has been reported that the optical properties of the perovskite nanocrystals can be controlled by either varying the halide ion composition or by changing the thickness of the nanocrystals.[35] This would enable the realization of perovskite-based actively tunable multifunctional metadevices.[36,37] Moreover, the thickness of solution processed perovskite coating can be easily controlled by spin coating and it can also be removed to restore the original response of the metamaterials.

IV. SUMMARY

In summary, we demonstrated high-*Q* plasmonic resonances in metal-dielectric-metal absorber cavity consisting of an array of conductively coupled annular and rectangular apertures that supports fundamental and higher order plasmonic resonances. Both the in-plane coupling between the resonators and the out of plane coupling between the resonators and metallic ground plane have been investigated to tailor the infrared response of the metamaterial absorber sensor. We have shown that the metamaterial absorber resonances can be precisely engineered by tailoring the coupling strength between the resonators, to enhance the sensitivity levels of the extremely weak and strong vibrational modes of the $CH_3NH_3PbI_3$ perovskite to a detectable level which are otherwise unidentifiable in the reflection spectra of an ultrathin film $CH_3NH_3PbI_3$. The high-*Q* fundamental dipolar and Fano resonances excited in the metamaterial enable infrared sensing of vibrational modes in extremely low volume analytes. These could also facilitate the design of novel tunable metamaterials, microcavity detectors, and thermal imaging devices. The extraordinary optical properties of perovskites and the advancement of the field of solution-processed fabrication technology distinguishes this new class of material as a leading candidate for next-generation active metadevices.

SUPPLEMENTARY MATERIAL

See supplementary material for method of fabrication, characterization, and simulation.

ACKNOWLEDGMENTS

Financial support from the Ministry of Education Academic Research Fund Tier 1 grants RG101/15 and RG173/16 and Tier 2 grants MOE2015-T2-2-015, MOE2015-T2-2-103, and MOE2016-T2-1-034 is gratefully acknowledged.

[1]S. A. Maier, *Plasmonics: Fundamentals and Applications* (Springer-Verlag, New York, 2007).
[2]S. Enoch and N. Bonod, *Plasmonics: From Basics to Advanced Topics* (Springer, Berlin, 2012).
[3]J. M. Pitarke, V. M. Silkin, E. V. Chulkov, and P. M. Echenique, Rep. Prog. Phys. **70**, 1–87 (2007).
[4]S. Link and M. A. El-Sayed, Int. Rev. Phys. Chem. **19**, 409–453 (2000).
[5]V. Giannini, A. I. Fernández-Domínguez, S. C. Heck, and S. A. Maier, Chem. Rev **111**, 3888 (2011).
[6]B. Luk'yanchuk, N. I. Zheludev, S. A. Maier, N. J. Halas, P. Nordlander, H. Giessen, and C. T. Chong, Nat. Mater. **9**, 707–715 (2010).
[7]A. E. Miroshnichenko, S. Flach, and Y. S. Kivshar, Rev. Mod. Phys. **82**, 2257–2298 (2010).
[8]V. A. Fedotov, M. Rose, S. L. Prosvirnin, N. Papasimakis, and N. I. Zheludev, Phys. Rev. Lett. **99**, 147401 (2007).
[9]W. R. Holland and D. G. Hall, Phys. Rev. Lett. **52**, 1041 (1984).
[10]A. B. Khanikaev, C. Wu, and G. Shvets, Nanophotonics **2**, 247 (2013).
[11]C. Ciracì, R. T. Hill, J. J. Mock, Y. Urzhumov, A. I. Fernández-Domínguez, S. A. Maier, J. B. Pendry, A. Chilkoti, and D. R. Smith, Science **337**, 1072 (2012).
[12]Y. Todorov, A. M. Andrews, I. Sagnes, R. Colombelli, P. Klang, G. Strasser, and C. Sirtori, Phys. Rev. Lett. **102**, 186402 (2009).
[13]C. M. Watts, X. Liu, and W. J. Padilla, Adv. Mater. **24**, OP98 (2012).
[14]G. Zheng, H. Mühlenbernd, M. Kenney, G. Li, T. Zentgraf, and S. Zhang, Nat. Nanotechnol. **10**, 308 (2015).
[15]J. Lee, M. Tymchenko, C. Argyropoulos, P.-Y. Chen, F. Lu, F. Demmerle, G. Boehm, M.-C. Amann, A. Alu, and M. A. Belkin, Nature **511**, 65–69 (2014).
[16]S. Guddala and S. A. Ramakrishna, Opt. Lett. **41**(22), 5150–5153 (2016).
[17]Z. Li, S. Butun, and K. Aydin, ACS Nano **8**, 8242–8248 (2014).
[18]N. I. Landy, S. Sajuyigbe, J. J. Mock, D. R. Smith, and W. J. Padilla, Phys. Rev. Lett. **100**, 207402 (2008).
[19]A. Moreau, C. Ciraci, J. J. Mock, R. T. Hill, Q. Wang, B. J. Wiley, A. Chilkoti, and D. R. Smith, Nature **492**, 86–89 (2012).
[20]L. Cong, S. Tan, R. Yahiaoui, F. Yan, W. Zhang, and R. Singh, Appl. Phys. Lett. **106**, 031107 (2015).
[21]E. J. R. Vesseur, F. J. García de Abajo, and A. Polman, Nano Lett. **9**, 3147–3150 (2009).
[22]G. Dayal, X. Y. Chin, C. Soci, and R. Singh, Adv. Opt. Mater. **4**, 1295–1301 (2016).
[23]W. Zhang, G. E. Eperon, and H. J. Snaith, Nat. Energy **1**, 16048 (2016).
[24]T. M. Brenner, D. A. Egger, L. Kronik, G. Hodes, and D. Cahen, Nat. Rev. Mater. **1**, 15007 (2016).
[25]B. R. Sutherland and E. H. Sargent, Nat. Photonics **10**, 295–302 (2016).
[26]M. B. Johnston, Nat. Photonics **9**, 634–636 (2015).
[27]B. Gholipour, G. Adamo, D. Cortecchia, H. N. S. Krishnamoorthy, M. Birowosuto, N. I. Zheludev, and C. Soci, Adv. Mater. **29**, 1604268 (2017).
[28]M. A. Pérez-Osorio, R. L. Milot, M. R. Filip, J. B. Patel, L. M. Herz, M. B. Johnston, and F. Giustino, J. Phys. Chem. C **119**, 25703 (2015).
[29]T. Glaser, C. Müller, M. Sendner, C. Krekeler, O. E. Semonin, T. D. Hull, O. Yaffe, J. S. Owen, W. Kowalsky, A. Pucci, and R. Lovrincič, J. Phys. Chem. Lett. **6**, 2913 (2015).
[30]R. Aroca, *Surface-Enhanced Vibrational Spectroscopy* (J. Wiley & Sons, Chichester, 2006).
[31]F. Neubrech, A. Pucci, T. W. Cornelius, S. Karim, A. GarcáEtxarri, and J. Aizpurua, Phys. Rev. Lett. **101**, 157403 (2008).
[32]C. Huck, J. Vogt, M. Sendner, D. Hengstler, F. Neubrech, and A. Pucci, ACS Photonics **2**(10), 1489 (2015).
[33]G. Dayal, X. Y. Chin, C. Soci, and R. Singh, Adv. Opt. Mater. **5**, 1600559 (2017).
[34]T. Neuman, C. Huck, J. Vogt, F. Neubrech, R. Hillenbrand, J. Aizpurua, and A. Pucci, J. Phys. Chem. C **119**, 26652 (2015).
[35]V. A. Hintermayr, A. F. Richter, F. Ehrat, M. Döblinger, W. Vanderlinden, J. A. Sichert, Y. Tong, L. Polavarapu, J. Feldmann, and A. S. Urban, Adv. Mater **28**, 9478 (2016).
[36]M. Manjappa, Y. K. Srivastava, A. Solanki, A. Kumar, T. C. Sum, and R. Singh, Adv. Mater. **2017**, 1605881.
[37]L. Cong, Y. K. Srivastava, A. Solanki, T. C. Sum, and R. Singh, ACS Photonics **4**(7), 1595–1601 (2017).